Available online at www.sciencedirect.com
ScienceDirect
Polymer 48 (2007) 3367–3376
polymer
www.elsevier.com/locate/polymer

Micro-mechanical model of TPE made of polypropylene and rubber waste

G. Ausias [a,*], S. Thuillier [a], B. Omnès [a], S. Wiessner [b,c], P. Pilvin [a]

[a] LG2M – Université de Bretagne-Sud, Mechanical Engineering, Rue de Saint-Maudé, BP 92116, F-56321 Lorient Cedex, Bretagne, France
[b] Kunststofftechnik, Institut für Allgemeinen Maschinenbau und Kunststofftechnik, Technische Universität Chemnitz (TUC), Reichenhainer Strasse 70, Zi. D 19, D-09126 Chemnitz, Germany
[c] Leibniz-Institute of Polymer Research Dresden e.V., Hohe Str. 6, D-01069 Dresden, Germany

Received 16 November 2006; received in revised form 19 March 2007; accepted 20 March 2007
Available online 24 March 2007

Abstract

The aim of this study is to conduct experimental characterization and to develop a micro-mechanical model for thermoplastic elastomers made of polypropylene and particles of rubber waste. Observations by means of Scanning Electron Microscope showed that the elastomer particles have an average dimension of 250 μm and are embedded in a polypropylene matrix. The mechanical behaviour is studied through a series of tensile tests composed of loadings at different strain rates and relaxation steps. The constitutive equations were established within a self-consistent scheme including the mechanical behaviour of the two phases. The matrix is modelled as an elastoviscoplastic solid and the rubber as an elastic solid. Material coefficients have been determined using an inverse method. This paper presents a first version of the micro-mechanical model and a comparison with experimental results.

Keywords: Micro-mechanical modelling; Thermoplastic elastomer; Constitutive behaviour

1. Introduction

A large quantity of rubber products, such as tyres, hoses and belts are consumed in Europe every year. Since they consist of irreversible cross-linked elastomers they cannot be remoulded as thermoplastics. Thus other ways of recycling of post-consumer elastomer products have to be applied. One possibility is to grind the rubber by several established milling procedures to obtain fine rubber particles [1] which can be used as functional fillers in polymeric matrices, for example polypropylene (PP) or polyethylene (PE) to obtain a thermoplastic elastomer (TPE). However, to achieve a good mechanical performance and TPE-like properties of the compounds a sufficient phase interaction at the interface between rubber inclusions and matrix is a necessity. This can be induced by radical reaction in the melt-mixing process [2]. TPEs based on rubber waste were developed in the 1990s and previous studies have shown that their mechanical properties are comparable to that of commercially available TPEs [3,4]. However, to make the material valuable for industrial applications, these mechanical properties must be described by models which in turn can be used by designers to predict the in-use behaviour.

The semi-crystalline thermoplastic matrix, itself, can be considered a complex material; therefore, several studies have developed models which take into account both a crystalline phase and an amorphous phase. For example, Van Dommelen et al. [5] proposed a multiscale numerical model to establish links between microscopic, mesoscopic, and macroscopic levels. While Bédoui et al. [6,7] developed two different models for the Young's modulus of semi-crystalline polymers. One was a differential scheme in which ellipsoidal crystallites were randomly dispersed in an amorphous matrix while the other was a self-consistent scheme in which the material was considered as an aggregate of randomly oriented two-layered

* Corresponding author. Tel.: +33 2 97880534; fax: +33 2 97880551.
E-mail address: gilles.ausias@univ-ubs.fr (G. Ausias).

0032-3861/$ - see front matter © 2007 Elsevier Ltd. All rights reserved.
doi:10.1016/j.polymer.2007.03.049

phase composite inclusions (crystalline–amorphous). For small deformations of semi-crystalline polymers, Nikolov et al. [8,9] presented a multiscale constitutive model in which micro-mechanically based constitutive equations were developed for each phase. They used a viscoplastic model for the crystalline lamellae and a new non-linear viscoelastic model for the amorphous phase behaviour. Moreover, Ahzi et al. [10] proposed a constitutive elastoviscoplastic model for the finite deformation stress–strain behaviour of poly(ethylene terephthalate) in which the crystallization rate evolves with the strain rate and the temperature. Similarly, they also put forward a two-phase self-consistent model for large deformation stress–strain behaviour and strain induced crystallization in polymers at temperatures above the glass transition temperature [11]. Crystallization under elongation has been measured in situ and seems to be a major factor in thermoplastic mechanical behaviour [12]. However, as a starting point, PP matrix will be considered as one mechanical phase in the present study.

Even though TPE structure complexity induces complex material processing and complex mechanical behaviour, models can be phenomenological and generally made of an assembly of simple mechanical elements such as springs and dash-pots [13]. For example, Veenstra et al. [14] developed a model for a polymer blend in which the co-continuous morphology was rendered by three orthogonal bars of a component embedded in a unit cube, the remaining volume of which was occupied by another component. Furthermore, this model was successfully used by Sengers et al. [15] to model TPE behaviour in dynamic solicitations.

Another way to build a model is to take into account the behaviour of each constituent, e.g. within a self-consistent scheme. For linear elasticity, Eshelby [16] established an analytical model. Indeed, several authors have proposed a linearization of the material behaviour by different techniques. A model for elastoviscoplastic material was established by Masson and Zaoui [17] who linearized the problem which was then solved by using a Laplace transform technique. Also, Molinari et al. [18] proposed an interaction law for isotropic behaviour and its validation [19]. The self-consistent method has often been used for metallic materials [20] but rarely for polymeric materials [21].

The number of phases in the model is linked to the level of complexity of the material and of the model. Chabert et al. [21] presented a homogenization method based on generalized self-consistent schemes to model polymer-based nanocomposite behaviour using different structure patterns. For a silica filled SBR, Mélé et al. [22] defined three phases: silica particles, bound rubber (the rubber close to the particle), and unbound rubber. The choice of the representative morphological pattern depends on the particle content. Their self-consistent model made with the viscoelastic properties of the different phases forwards the better understanding of the viscoelastic behaviour of the material. The Finite Element Method (FEM) is sometimes used to calculate stresses and strains in the Representative Volume Element (RVE) containing one [23] or several inclusions with different sizes in random positions for soft inclusions [24] or rigid particles for a nanocomposite [25]. FEM could also be used to validate a self-consistent model [19]. In a composite like TPE, soft particles are greatly stretched at very large deformation and Asami and Nitta [26] have studied these particle deformations under large strains using Scanning and Transmission Electron Microscopes, as well as Finite Element Method simulation.

In this study, a self-consistent scheme is used to create a model for the description of the mechanical behaviour of thermoplastic elastomers consisting of a polypropylene matrix with dispersed elastomer inclusions, i.e. forming an island-matrix structure. Indeed, the ability to understand and describe the material behaviour provides the possibility to model the service behaviour of products or parts made of these materials such as car bumpers [27] or rubber boots [28]. And also to model the material behaviour during some processing operations, as for instance stamping [29] or forming of solid polymers [30]. As a first step, quasi-static tests within a moderate strain range and relaxation tests were chosen, as a car bumper loading. A new model is proposed with a suitable scale transition rule from the macroscopic level to the phase level. First of all, the material and the experimental tests are presented. Then, the micro-mechanical model is detailed, as well as the constitutive law of the PP and the rubber. Model parameters are then identified by inverse method. Finally, the model results are compared to the experimental results.

2. Materials and experimental results

2.1. Materials

A commercial unfilled polypropylene (Basell, Moplen RP220M) was used as the matrix, and the elastomer particles of an average size of 250 μm originate from ground tread layers of truck tyres. To establish a good interaction between the two phases, a reactive melt-mixing process with the use of radical donators in the form of organic peroxides and, if required, radical acceptors as coagents, was developed [2,4]. This process was performed in an internal mixer. Electrical power consumption was recorded to control the blending process state. The PP matrix and elastomer powder were fed into the mixer, and once a homogeneous compound was obtained, the additives were added. To develop the model, three materials were studied: isotactic polypropylene (PP) and two TPEs (TPE45 and TPE65) with a rubber volume fraction of 0.45 and 0.65, respectively (containing 50 wt% and 70 wt% of rubber particles, respectively). Tensile test specimens with a cross-section area of (4×10) mm^2 were injection moulded. The micrographs in Fig. 1 show the phase morphology of the TPEs obtained with a Scanning Electron Microscope (SEM).

2.2. Tests

An Instron 5567 testing machine was used at room temperature for tensile tests. Strains were measured with an axial extensiometer, and mechanical behaviour was studied during

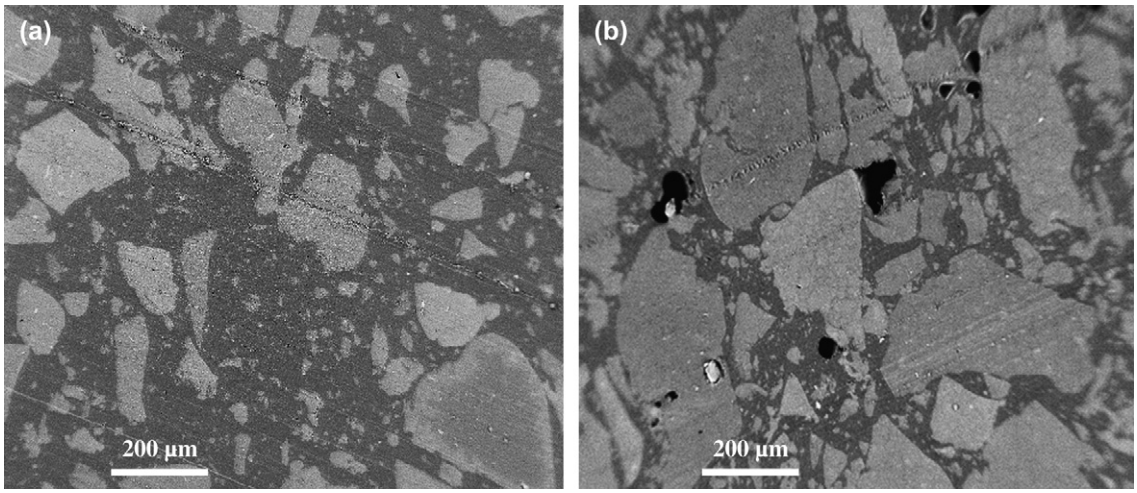

Fig. 1. Morphology of TPE45 (a) and TPE65 (b) observed by SEM. Elastomer particles appear pale grey and the matrix PP is dark. The black voids in (b) result from the sample preparation procedure.

loading–relaxation tests. Both axial strain and load were recorded during the test. By assuming an isochoric deformation [31] Cauchy stress was calculated, as well as logarithmic axial strain. An elastoviscoplastic model was chosen for the PP and a specific strain history with loading phases at different strain rates ($10^{-4}\,s^{-1}$, $10^{-3}\,s^{-1}$, $10^{-2}\,s^{-1}$) and relaxation phases (300 s) were tested to thoroughly identify the model. TPEs were tested with a loading phase at $5\times10^{-3}\,s^{-1}$ followed by a relaxation phase for 900 s. Fig. 2 gives the loading paths for the PP and the TPE.

3. Micro-mechanical modelling

3.1. Introduction

The first step is to determine the pertinent scale to describe the material structure. It mainly depends on the size of the biggest heterogeneities present in the material. An intermediate scale between the atomic scale and the scale of the considered structure must be chosen, and a Representative Volume Element (RVE) has to be defined. It must be larger than the biggest heterogeneities, yet small enough to respect the continuum mechanics hypothesis; a necessary condition to be able to consider that the RVE is representative would be that the average stress $\langle\boldsymbol{\sigma}\rangle$ and the average strain $\langle\boldsymbol{\varepsilon}\rangle$ over the RVE are equal, respectively, to the macroscopic stress $\boldsymbol{\Sigma}$ and to the macroscopic strain $\mathbf{E}$ as:

$$\boldsymbol{\Sigma} = \langle\boldsymbol{\sigma}\rangle = f_0\boldsymbol{\sigma}_0 + f_1\boldsymbol{\sigma}_1 \tag{1}$$

$$\mathbf{E} = \langle\boldsymbol{\varepsilon}\rangle = f_0\boldsymbol{\varepsilon}_0 + f_1\boldsymbol{\varepsilon}_1 \tag{2}$$

where f_k, $\boldsymbol{\sigma}_k$ and $\boldsymbol{\varepsilon}_k$ are the volume fraction, the stress and strain tensors, respectively, of phase k, while subscript indexes 0 and 1 represent the matrix and the filler, respectively. The brackets $\langle\rangle$ denote volume averages over all the volume. In this case, global RVE behaviour is assumed to be the same as that of a Homogeneous Equivalent Medium (HEM), similar to the heterogeneous material. Shapes, volume fractions, orientations of different phases have to be described, as well as their mechanical behaviours [21]. This description is generally simplified and incomplete; therefore, the model gives only an estimate of the real behaviour. The next step is then the localization step in which relations between global quantities and local quantities at position $\mathbf{x}$ have to be determined.

When the material is only understood by the phase volume fractions without any information on the morphology, Voigt and Reuss models can be used [32]. They provide upper and lower bounds, respectively, for the macroscopic behaviour. In the Reuss hypothesis, stress is uniform throughout the RVE which can be written as: $\boldsymbol{\Sigma} = \boldsymbol{\sigma}_0(\mathbf{x}) = \boldsymbol{\sigma}_1(\mathbf{x})$. In the Voigt hypothesis, strain is uniform throughout the RVE which can be written as:

$$\mathbf{E} = \boldsymbol{\varepsilon}_0(\mathbf{x}) = \boldsymbol{\varepsilon}_1(\mathbf{x}). \tag{3}$$

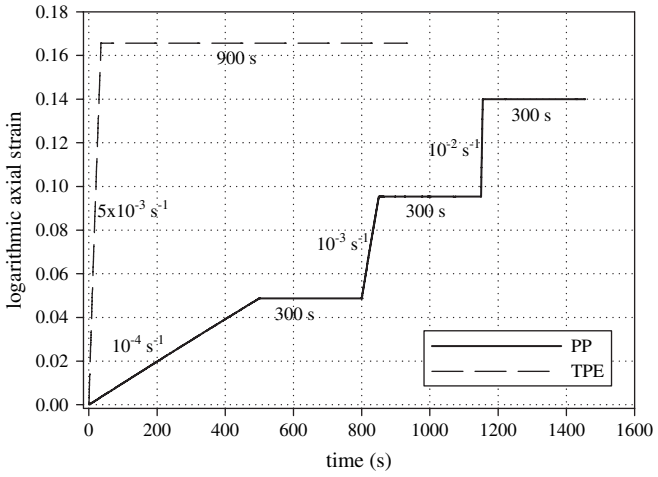

Fig. 2. Strain loading history for the PP and the TPEs. The strain rate and the relaxation duration are given for each step.

3.2. Linear elasticity

In linear elasticity, average stress tensor in the phases and the macroscopic strain is related to the macroscopic stress tensor by the stress concentration tensor $\mathcal{A}_k$ and the effective elastic tensor C_h, respectively, which are defined by the two following relations:

$$\boldsymbol{\sigma}_k = \mathcal{A}_k : \boldsymbol{\Sigma} \tag{4}$$

$$\mathbf{E} = C_h^{-1} : \boldsymbol{\Sigma} \tag{5}$$

To fulfil the stress average conditions (Eq. (1)), tensors $\mathcal{A}_k$ have to carry out the condition: $\sum_k f_k \mathcal{A}_k = I$ where I is the fourth-order identity tensor. Tensors $\mathcal{A}_k$ depend on the model chosen. They have been presented in detail by Nemat-Nasser and Hori [32] and by Mura [33]. For a material made with two phases, the fourth-order homogenized modulus tensor C_h can be calculated as:

$$C_h^{-1} = f_0 C_0^{-1} \mathcal{A}_0 + f_1 C_1^{-1} \mathcal{A}_1 \tag{6}$$

The self-consistent approach is an efficient tool to derive the global mechanical behaviour of aggregates from the mechanical behaviour of each phase. Some analytical models have been proposed for cases of linear isotropic elasticity [34]. The Classical Self-Consistent (CSC) method consists in successively setting phases in the HEM, while the Generalized Self-Consistent (GSC) method consists in simultaneously setting all phases in the RVE [34]. In the latter, different morphologies can be considered. With two phases, fillers (rubber) can be introduced in the matrix (GSC − RUBinPP) or the PP phase can be introduced in the rubber phase (GSC − PPinRUB). This second morphology can be considered if a very high rubber volume fraction above the maximum packing fraction is used, thus leading to a morphology formed by "agglomerated rubber particles with PP-filled interstices". The first step is to determine the best morphology with the Young's modulus calculation. Voigt and Reuss models, the Classical Self-Consistent (CSC) model, and the two Generalized Self-Consistent (GSC) models have been used to estimate the TPE modulus for rubber volume fractions between 0 and 1. For this calculation, knowledge of the Young's modulus and bulk modulus for both phases is required. The Young's modulus of the PP was obtained from the tensile tests. Poisson's ratio was taken from the literature with an estimated value of 0.4 [35]. Fig. 3 shows the calculated moduli versus rubber volume fraction according to the different models. The experimentally obtained moduli of PP, the TPE45 and the TPE65 (841 ± 41 MPa, 336 ± 54 MPa and 168 ± 18 MPa, respectively) are shown for comparison. These Young's moduli have been determined from tensile tests realised at a strain rate of $10^{-4}\ s^{-1}$. Since it was not possible to measure the modulus of the elastomer due to the nature as a powder the elastomer modulus must be chosen to fit the best experimental modulus. The best fit was obtained for the GSC − RUBinPP model and for an elastomer modulus consistent with the literature. Table 1 summarizes the Young's modulus and bulk modulus for the elastomer and for the PP. These results justify the choice of the morphological pattern made of dispersed fillers inside a continuous matrix (Fig. 4).

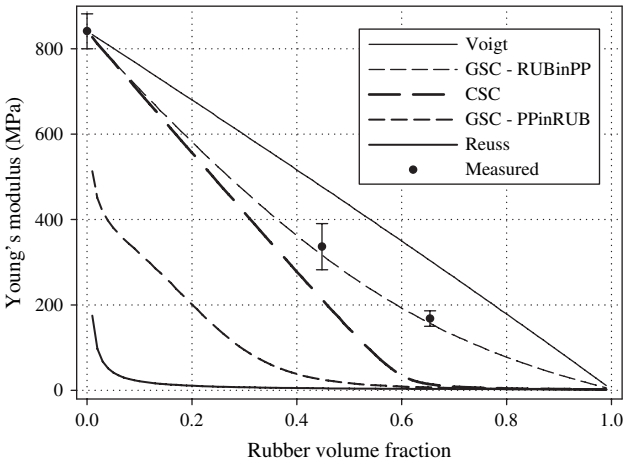

Fig. 3. Young's moduli measured on samples and calculated with the different models.

3.3. Non-linear behaviour

To extend the micro-mechanical model to higher strains, it is necessary to consider both the non-linear behaviour of the phases and a specific scale transition rule which takes into account the non-linear accommodation of stress heterogeneities between the phases. The large transformation framework and the non-linear behaviour of each phase are presented first and then the micro-mechanical model is detailed.

3.3.1. Large transformation framework

The use of local objective frames is now well established as an efficient method to develop constitutive models at finite strains, which automatically fulfil the material frame indifference requirement [36]. In this work, the corotational frame is defined at macroscopic level and is associated to the skew-symmetric part $\boldsymbol{\Omega}$ of the velocity gradient $\mathbf{L}$. Let $\mathbf{Q}_c$ be the rotation between the current space frame and the corotational frame, $\dot{\mathbf{Q}}_c \mathbf{Q}_c^t = \boldsymbol{\Omega}$. An additive decomposition of the strain rate tensor in the corotational frame can then be defined by:

$$\dot{\mathbf{E}} = \mathbf{Q}_c^t \mathbf{D} \mathbf{Q}_c = \dot{\mathbf{E}}^e + \dot{\mathbf{E}}^{in} \tag{7}$$

with the strain rate tensor $\mathbf{D} = \mathbf{L} + \boldsymbol{\Omega}$. $\dot{\mathbf{E}}^e$ and $\dot{\mathbf{E}}^{in}$ represent the elastic and the inelastic strain rates, respectively. Constitutive laws are written in the corotational frame, using the co-rotated Cauchy stress tensor defined by:

$$\boldsymbol{\Sigma} = (\det \mathbf{F}) \mathbf{Q}_c^t \mathbf{S} \mathbf{Q}_c \tag{8}$$

Table 1
Young's modulus and bulk modulus for the elastomer and for the PP

Coefficient	E_0 (MPa)	K_0 (MPa)	E_1 (MPa)	K_1 (MPa)
Value	840	1400	3.0	1250

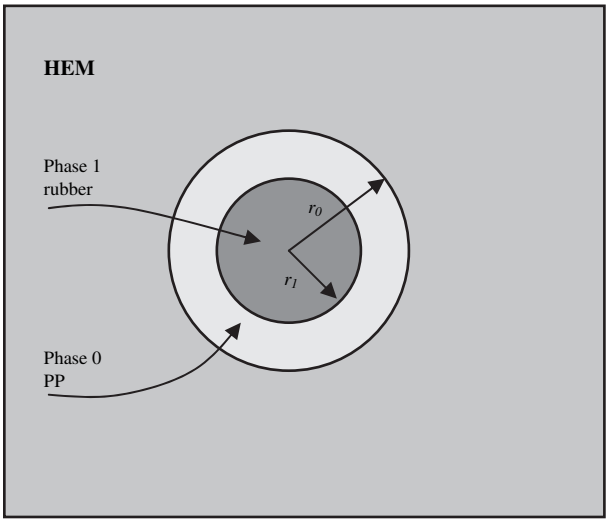

Fig. 4. Sketch of the chosen morphological pattern for generalized self-consistent model. The ratio r_1/r_0 is related to the rubber volume fraction.

with **F** the transformation gradient tensor and **S** the Cauchy stress tensor. The associated derivative is then the Jaumann derivative. Each phase is assumed to rotate the same way as the HEM. Therefore, microscopic stress and strain tensors are defined and calculated in the same corotational frame.

3.3.2. Phase behaviours

As previously mentioned, the thermoplastic matrix, itself, has a complex behaviour. For the present work, the micromechanical behaviour of the thermoplastic matrix was put aside and a phenomenological model has been used instead. Bruselle-Dupend et al. [13] proposed a phenomenological model to describe the mechanical behaviour of a polypropylene. The model developed here is an elastoviscoplastic analog system established from Bruselle-Dupend's model [13] and formed with a viscoelastic block acting in series with a viscoplastic block (Fig. 5). The strain $\boldsymbol{\varepsilon}_0$ in the PP is, therefore, expressed as the sum of a viscoelastic part ($\boldsymbol{\varepsilon}_0^{\mathrm{ve}}$) and a viscoplastic part ($\boldsymbol{\varepsilon}_0^{\mathrm{vp}}$):

$$\boldsymbol{\varepsilon}_0 = \boldsymbol{\varepsilon}_0^{\mathrm{ve}} + \boldsymbol{\varepsilon}_0^{\mathrm{vp}} \tag{9}$$

First, the viscoplastic contribution was developed within the framework of associated plasticity for a generalized standard material as defined by Lemaitre and Chaboche [37]. We first have to introduce a function F which depends on the stress tensor $\boldsymbol{\sigma}_0$ and a non-linear kinematic variable **X** such as [31]:

$$F(\boldsymbol{\sigma}_0, \mathbf{X}) = J_2(\boldsymbol{\sigma}_0 - \mathbf{X}) - \sigma_y + \frac{1}{4\sigma_y} J_2^2(\mathbf{X}) \tag{10}$$

where σ_y represents the initial yield stress and J_2 represents the von Mises equivalent of a tensor. The last term has been added to model the elastic domain decrease. This term has been proposed by Ladeveze and Rougee [38]. $\boldsymbol{\varepsilon}_0^{\mathrm{vp}}$ follows a normality flow rule (Eq. (11)) derived from a viscoplastic potential $\Omega(F)$, such that $\Omega'(F)$ is given by Eq. (12) [31].

$$\dot{\boldsymbol{\varepsilon}}_0^{\mathrm{vp}} = \frac{\partial \Omega}{\partial \boldsymbol{\sigma}_0} = \frac{\partial \Omega}{\partial F}\frac{\partial F}{\partial \boldsymbol{\sigma}_0} \tag{11}$$

$$\Omega'(F) = \frac{\partial \Omega}{\partial F} = \dot{\varepsilon}_0 \sinh\left(\frac{F}{N}\right) \tag{12}$$

Finally, the evolution of $\boldsymbol{\varepsilon}_0^{\mathrm{vp}}$ can be expressed as:

$$\begin{cases} \dot{\boldsymbol{\varepsilon}}_0^{\mathrm{vp}} = 0 \quad \text{if} \quad F \le 0 \\ \dot{\boldsymbol{\varepsilon}}_0^{\mathrm{vp}} = \dfrac{\partial \Omega}{\partial \overline{\boldsymbol{\sigma}}_0} = \dfrac{3}{2}\dfrac{\overline{\boldsymbol{\sigma}}_0 - \mathbf{X}}{J_2(\overline{\boldsymbol{\sigma}}_0 - \mathbf{X})}\Omega'(F) \quad \text{if} \quad F > 0 \end{cases} \tag{13}$$

Hardening is purely kinematic but the size of the yield stress surface will vary according to the last term of the right-hand side term of Eq. (10). The evolution law of $\boldsymbol{\alpha}$ is derived from:

$$-\dot{\boldsymbol{\alpha}} = \frac{\partial \Omega}{\partial \mathbf{X}} \quad \text{where } \mathbf{X} = \frac{2}{3} C \boldsymbol{\alpha} \tag{14}$$

which can be summarized as:

$$\dot{\boldsymbol{\alpha}} = \dot{\boldsymbol{\varepsilon}}_0^{\mathrm{vp}} - \frac{C}{2\sigma_y}\Omega'(F)\boldsymbol{\alpha} \tag{15}$$

Let us now consider the viscoelastic block. It is split into two parallel parts (Fig. 5). The first one (index a) is elastic and characterized by its fourth-order elastic tensor C_a. The second one (index b) is viscoelastic and characterized by its fourth-order elastic tensor C_b. The elastic properties are assumed to be isotropic and characterized by the Young's moduli E_a and E_b, and the compressibility moduli K_a and K_b. In order to simplify the equations, it is assumed that their Poisson's ratios are equal. This assumption leads to a simplification of the constitutive equations. Let us now define the total elastic tensor such that: $C_0 = C_a + C_b$. The stress tensor is related to the strain tensor by $\boldsymbol{\sigma}_0 = C_0 : (\boldsymbol{\varepsilon}_0 - \boldsymbol{\varepsilon}_0^{\mathrm{in}})$ where $\boldsymbol{\varepsilon}_0^{\mathrm{in}} = C_0^{-1} C_b : \boldsymbol{\varepsilon}_b + \boldsymbol{\varepsilon}_0^{\mathrm{vp}}$. In this work, $\boldsymbol{\varepsilon}_0^{\mathrm{vp}}$ represents the strain of the viscoplastic block and $\boldsymbol{\varepsilon}_0^{\mathrm{in}}$ represents the total inelastic strain of the PP. $\boldsymbol{\varepsilon}_b$ is the viscoelastic strain part of the viscous element. The evolution law of $\boldsymbol{\varepsilon}_b$ is given by:

$$\dot{\boldsymbol{\varepsilon}}_b = \left(\frac{J_2(\boldsymbol{\sigma}_b)}{\eta_b}\right)^n \frac{\overline{\boldsymbol{\sigma}}_b}{J_2(\boldsymbol{\sigma}_b)} \tag{16}$$

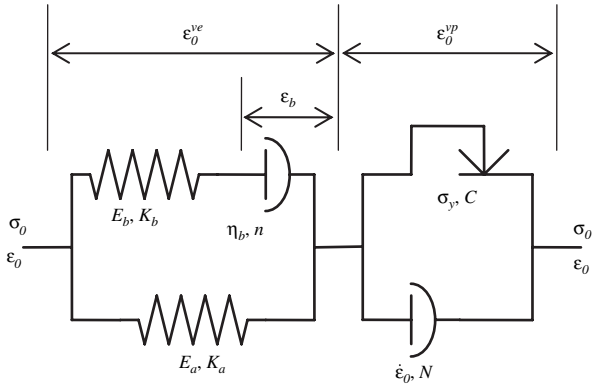

Fig. 5. Sketch of PP model.

with $\boldsymbol{\sigma}_b = C_0^{-1} C_b : (\boldsymbol{\sigma}_0 - C_a : \boldsymbol{\varepsilon}_b)$. $\overline{\boldsymbol{\sigma}}_b$ the deviatoric part of $\boldsymbol{\sigma}_b$. η_b and n are two material parameters.

Assuming that the bulk modulus of the PP is known, this model has eight parameters to be determined from tensile tests. Table 2 summarizes the values obtained, whereas Figs. 6 and 7 give Cauchy stress versus logarithmic axial strain and time, respectively, in a loading test at a strain rate of $5 \times 10^{-4}\,s^{-1}$ followed by a relaxation step, which demonstrates that this model leads to correct representation of the mechanical behaviour during load and relaxation steps.

The behaviour of the rubber powder is assumed to be purely linear elastic and isotropic, and defined by a Young's modulus and a bulk modulus. This assumption seems to be correct for a limited strain range. The elastomer is assumed to be incompressible (Table 1). The Young's modulus of the particles will be determined in a second step by inverse identification method over the composite because particles are too small to be characterized directly.

3.3.3. The β model

In order to illustrate the extension of self-consistent models to large-strain framework and non-linear constitutive behaviour, the Voigt model is considered in the first step. Inelastic behaviour of the phases can be written as:

$$\boldsymbol{\sigma}_k = C_k : (\boldsymbol{\varepsilon}_k - \boldsymbol{\varepsilon}_k^{\text{in}}) \tag{17}$$

where C_k is the fourth-order elastic tensor and $\boldsymbol{\varepsilon}_k^{\text{in}}$ is the inelastic strain tensor for phase k. In the case of the Voigt model, the strain tensor is uniform throughout the phases and equal to the macroscopic strain tensor (Eq. (3)). The macroscopic stress tensor can also be written as:

$$\boldsymbol{\Sigma} = C_h : \left(\mathbf{E} - \mathbf{E}^{\text{in}}\right) \tag{18}$$

with $C_h = \sum_k f_k C_k$ and

$$\mathbf{E}^{\text{in}} = {}^{v}C_h^{-1} : \left(\sum_k f_k C_k : \boldsymbol{\varepsilon}_k^{\text{in}}\right) \tag{19}$$

where ${}^{v}C_h$ is the homogenized modulus tensor in the particular case of the Voigt hypothesis. Therefore, from Eq. (17), the Voigt model can be expressed for non-linear behaviour as:

$$\boldsymbol{\sigma}_k = {}^{v}\mathcal{A}_k : \left[\boldsymbol{\Sigma} + {}^{v}C_h : \left(\mathbf{E}^{\text{in}} - \boldsymbol{\varepsilon}_k^{\text{in}}\right)\right] \tag{20}$$

where ${}^{v}\mathcal{A}_k$ is the strain concentration tensor of phase k in the particular case of the Voigt hypothesis.

Among self-consistent models, one has been chosen which has been already successfully used for metallic alloys [36,39–41]. In this model which can be seen as an extension of

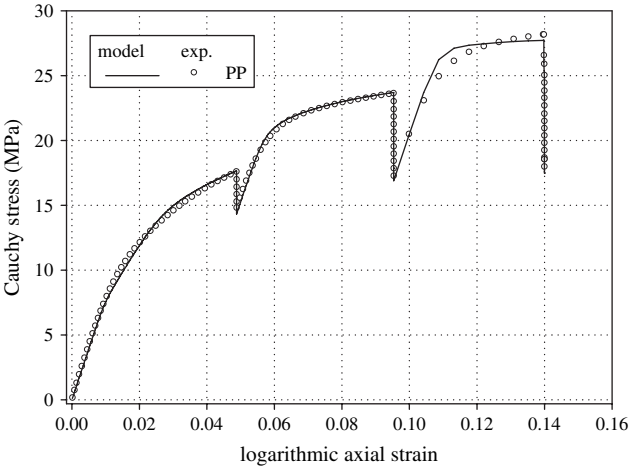

Fig. 6. Cauchy stress versus logarithmic axial strain for the PP.

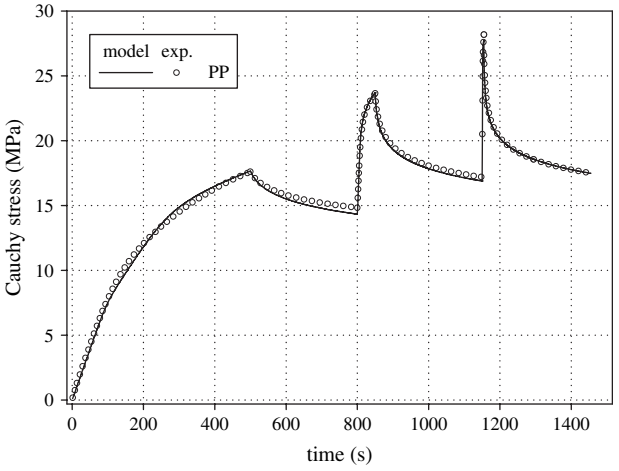

Fig. 7. Cauchy stress versus time for the PP.

Eq. (20), the local inelastic strain $\boldsymbol{\varepsilon}_k^{\text{in}}$ is replaced by a phenomenological variable $\boldsymbol{\beta}_k$ and the local stress tensor is written as:

$$\boldsymbol{\sigma}_k = \mathcal{A}_k : [\boldsymbol{\Sigma} + \mathcal{D}_k : (\mathbf{B} - \boldsymbol{\beta}_k)] \tag{21}$$

$\boldsymbol{\beta}_k$ presents a non-linear evolution with respect to plastic strain. They are called inter-phase accommodation variables. $\mathbf{B}$ and $\boldsymbol{\beta}_k$ are defined with respect to the corotational frame and are, thus, respect the material frame indifference. The initial values of these tensors are equal to zero and their time evolutions can be written as:

$$\dot{\boldsymbol{\beta}}_k = \dot{\boldsymbol{\varepsilon}}_k^{\text{in}} - D_k \boldsymbol{\beta}_k \left\| \dot{\boldsymbol{\varepsilon}}_k^{\text{in}} \right\| \tag{22}$$

The time evolutions depend on the inelastic strain rate tensor and for this reason in the present study, as the elastomeric

Table 2
Coefficients for the PP

Coefficient	E_a (MPa)	E_b (MPa)	η_a (MPa s)$^{1/n}$	N	C (MPa)	N	σ_y (MPa)	$\dot{\varepsilon}_0$ (s^{-1})
Value	423	362	10.9	8.19	240	1.45	6.22	0.326×10^{-6}

phase is considered to be completely elastic, $\boldsymbol{\beta}_1$ remains equal to zero. D_0 is a tuning parameter which will be identified later. Replacing total strain by $\mathbf{B}$ assumes that the main source of heterogeneities is plasticity more than elasticity. This new variable was shown to correctly capture the plastic accommodation which comes from the self-consistent formalism [41,42]. The tensor $\mathbf{B}$ has to respect the stress average condition in the volume. Using Eqs. (1) and (21) it can be expressed as:

$$\mathbf{B} = (f_0\mathcal{A}_0\mathcal{D}_0 + f_1\mathcal{A}_1\mathcal{D}_1)^{-1}(f_0\mathcal{A}_0\mathcal{D}_0 : \boldsymbol{\beta}_0 + f_1\mathcal{A}_1\mathcal{D}_1 : \boldsymbol{\beta}_1), \quad (23)$$

We consider that the phases exhibit isotropic behaviour and in this case the tensor $\mathcal{D}_k$ can be written as:

$$\mathcal{D}_k = (a_k\mathcal{K} + b_k\mathcal{J})C_h \quad (24)$$

with $\mathcal{K} = \mathbf{I} \times \mathbf{I}$ and $\mathcal{J} = I - \mathcal{K}$. $\mathbf{I}$ represents the second-order unity tensor. Furthermore, the Voigt and Reuss models are two particular cases of this model which tends to the Voigt model for $\mathcal{A}_k = C_k{}^{\mathcal{V}}C_h^{-1}$ and $\mathcal{D}_h = {}^{\mathcal{V}}C_h(a_k = 1,\ b_k = 1)$, and to the Reuss model for $\mathcal{A}_k = I$ and $\mathcal{D}_k = 0(a_k = 0, b_k = 0)$. To complete the model, the macroscopic inelastic strain, $\mathbf{E}^{\text{in}}$ has to be defined. From Eqs. (2), (17) and (18), $\mathbf{E}^{\text{in}}$ can be written as:

$$\mathbf{E}^{\text{in}} = f_0\boldsymbol{\varepsilon}_0^{\text{in}} + f_1\boldsymbol{\varepsilon}_1^{\text{in}} + f_0C_0^{-1}\mathcal{A}_0\mathcal{D}_0 : (\mathbf{B} - \boldsymbol{\beta}_0) + f_1C_1^{-1}\mathcal{A}_1\mathcal{D}_1 : (\mathbf{B} - \boldsymbol{\beta}_1) \quad (25)$$

Eqs. (23) and (25) have been presented in a general form. They could be simplified in this study considering that the rubber exhibits elastic behaviour. In this case $\boldsymbol{\varepsilon}_1^{\text{in}} = 0$ and $\boldsymbol{\beta}_1 = 0$. Then, the macroscopic stress can be calculated using Eq. (18). The model used in this work is described by the set of Eqs. (16)–(25) with three tuning coefficients b_0, b_1 and D_0.

3.4. Finite Element Method (FEM) simulation and Self-Consistency Conditions (SCC)

The model is able to calculate stress and strain tensors in the two phases, as well as for the homogenized material, however, no analytical solution exists for the inclusion problem when the behaviour is non-linear. The model has been assessed by means of a Finite Element Method (FEM) calculation, and its overall behaviour of the model is compared to the FEM model using volume averages of stress and strain. The ABAQUS software was used, in the same way as Mercier et al. [19] used it to model the behaviour of the pattern. In order to reduce calculation time, FEM analysis has been performed with the 2D axisymmetric assumption. Only an eighth of the geometry has been represented (Fig. 4). Inner, intermediate, and outer areas represent the rubber, the polypropylene, and the HEM, respectively. They were modelled with 21, 12, and 42 elements, respectively. 8-Node bilinear elements with reduced integration were used. The volume of rubber and PP is equal and this mesh models a TPE with 50% volume fraction of rubber (TPE50). The model has been implemented in a user subroutine UMAT in ABAQUS. Rubber, PP, and the HEM behaviours are described by the model for 100%, 0%, and 50% of rubber volume fractions, respectively. The lower surface is a plane of symmetry and the solicitation has been applied to the upper surface. Boundary conditions are represented in Fig. 8. The traction vector is continuous at the interface; perfect bonding is assumed. The stress average in each phase has been computed and compared to the stress calculated with the model [19,41]. The self-consistency conditions can be expressed with the following proposition:

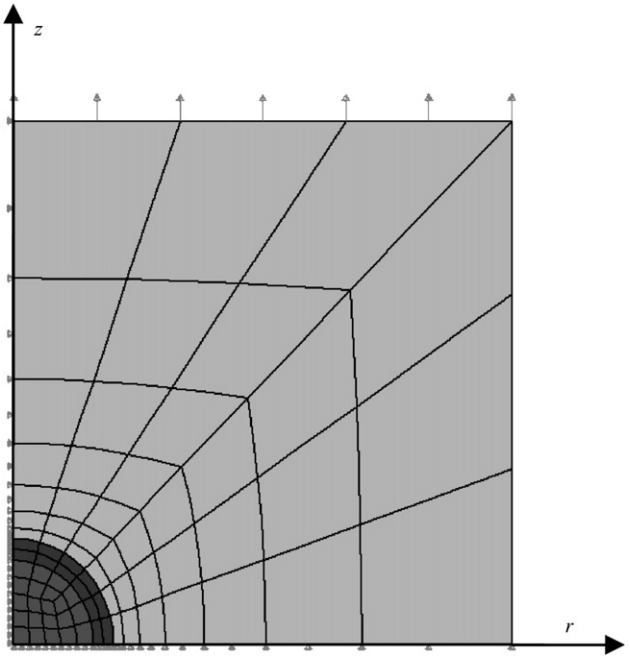

Fig. 8. Mesh of the pattern and the boundary conditions.

$$\forall g \in \mathcal{W},\ \forall t,\ \langle\boldsymbol{\sigma}_k^{\text{FEM}}\rangle - \boldsymbol{\sigma}_k^{\text{model}} = 0,\ \langle\boldsymbol{\varepsilon}_k^{\text{FEM}}\rangle - \boldsymbol{\varepsilon}_k^{\text{model}} = 0,\ \forall k \quad (26)$$

where w is the set of numerical experiments. $\langle\boldsymbol{\sigma}_k^{\text{FEM}}\rangle$ and $\langle\boldsymbol{\varepsilon}_k^{\text{FEM}}\rangle$ represent the average stress tensor and the average strain tensor, respectively, in phase k calculated by the Finite Element Method calculation within the volume of phase k. $\boldsymbol{\sigma}_k^{\text{model}}$ and $\boldsymbol{\varepsilon}_k^{\text{model}}$ represent the stress and strain tensors, respectively, calculated with the model.

4. Results

4.1. Parameter identification

The set of parameters, denoted $\mathbf{A}$, of the model are identified by a quantitative comparison of the experimental observations $\mathbf{Z}^{\text{exp}}$ and the modelled simulations of these experiments $\mathbf{Z}^{\text{model}}$. This identification task is classically expressed by an optimization problem based on the cost function defined by:

$$\mathcal{L}(\mathbf{A}) = \sum_{j\in\mathcal{V}} \int_{t\in I_j} \left|\mathbf{Z}^{\text{exp}}(t) - \mathbf{Z}^{\text{model}}(\mathbf{A}, t)\right| \mathrm{d}t \quad (27)$$

where the symbol $|\bullet|$ represents a dimensionless norm on the space of the observable variables (strain, displacement,

load,…) and I_j the observation interval in the jth test of the experimental base $\mathcal{V}$. For the proposed model, the parameters $\mathbf{A}$ have to be determined from tensile test results and the self-consistent conditions of the homogenization process. The identification method has therefore been modified to take these conditions into account. A penalty term has been introduced in the cost function in order to limit the optimization process to these conditions. The self-consistency of the model is estimated by the comparison of the results of the boundary value calculated by the Finite Element Method simulation and those predicted by the model with the same loading paths. Therefore, the optimization problem can be expressed as the minimization of the following cost function:

$$\mathcal{L}_p(\mathbf{A}) = \mathcal{L}(\mathbf{A}) + \sum_{j\in\mathcal{W}} \sum_{k=1,2} \int_{t\in I_g} \Big\{ |\langle \boldsymbol{\sigma}_k^{\mathrm{FEM}} \rangle - \boldsymbol{\sigma}_k^{\mathrm{model}}| + |\langle \boldsymbol{\varepsilon}_k^{\mathrm{FEM}} \rangle - \boldsymbol{\varepsilon}_k^{\mathrm{model}}| \Big\} \mathrm{d}t \tag{28}$$

Localization law coefficients have been determined to minimize the differences between experimental results and direct simulation [43] on one hand, and between experimental results and FEM simulation on the other. In this study, only tensile tests have been realised and, therefore, the results are quasi-insensitive to hydrostatic pressure. In this case, a_i which controls the hydrostatic part of $\mathcal{D}_k$ has no effect on the model results and it cannot be determined in this work. They have been set equal to 1. The minimization of Eq. (28) has been done with the software SiDoLo [44]. This identification has given the parameter values summarized in Table 3.

4.2. Results

Figs. 9 and 10 show the comparison of experimental and calculated Cauchy stress versus logarithmic axial strain and time, respectively, for the two TPEs for a load at a constant strain rate of 0.001 s^{-1} followed by relaxation. The loading step has been correctly predicted, as well as the relaxation step which is exact when predicted by the model as for the PP. It can be concluded that the viscosity component of the rubber does not have a large effect on material behaviour for the range of strain rate studied. Stress tensor components in the rubber and in the PP have been compared using both the model and the FEM simulation. Fig. 11 shows Cauchy stress for a 50% volume fraction elastomer (TPE50) for a load at a constant strain rate of 0.001 s^{-1}, and Fig. 12 shows equivalent strain in the matrix (PP) and in the rubber (RUB) for the same previous test. Comparisons of model behaviour to FEM simulation have been conducted for different volume fractions of

Table 3
GSC − RUBinPP model parameter values

Coefficient	a_0	a_1	b_0	b_1	D_0
Value	1.0	1.0	0.4086	2.1432	0.0855

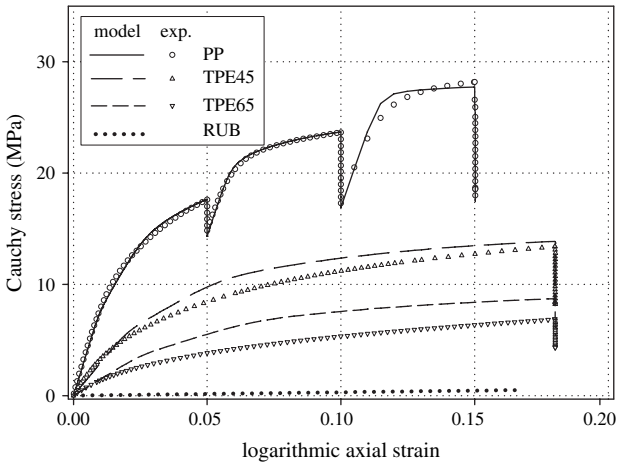

Fig. 9. Comparison of experimental and simulated Cauchy stress versus logarithmic axial strain for the two TPEs.

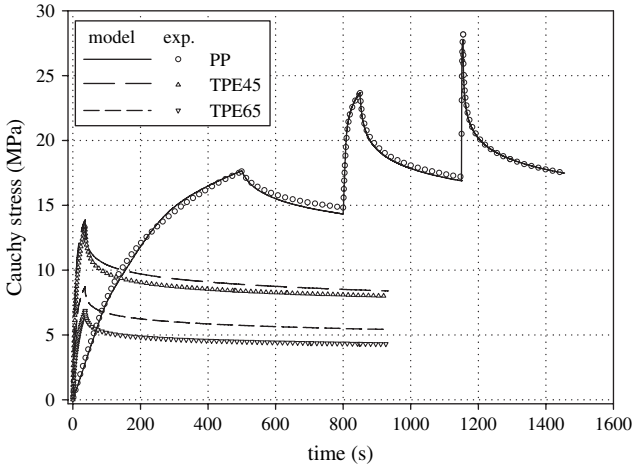

Fig. 10. Comparison of experimental and simulated Cauchy stress versus time for the two TPEs.

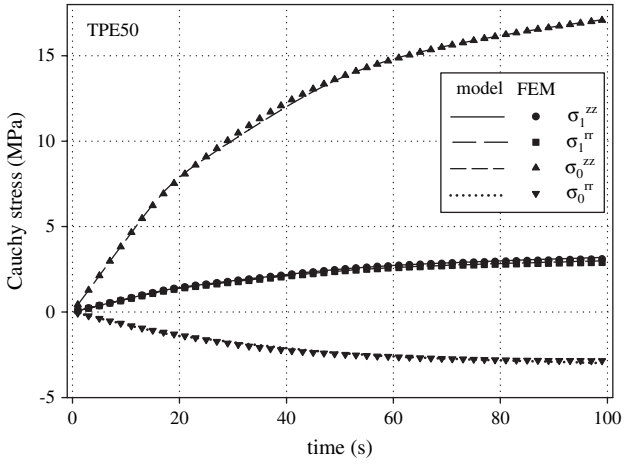

Fig. 11. Simulated Cauchy stress versus time for the TPE50 and in the two phases for a test of monotonic loading at $\dot{E}^{zz} = 10^{-3}\ s^{-1}$.

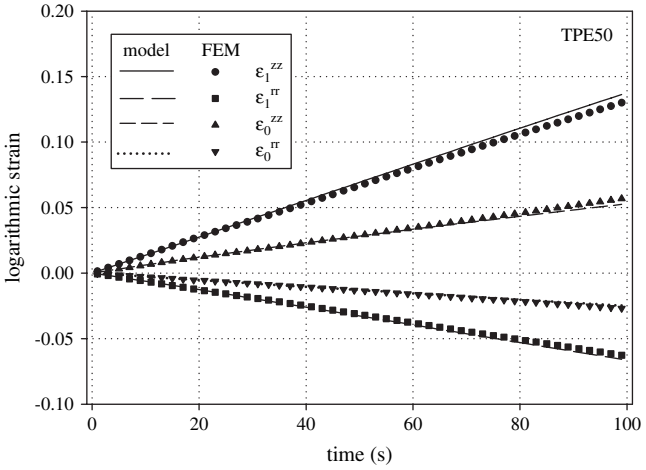

Fig. 12. Simulated logarithmic axial strain versus time for the TPE50 and in the two phases for a test of monotonic loading at $\dot{E}^{zz} = 10^{-3}\ s^{-1}$.

elastomer. Fig. 13 gives calculated axial stress in the PP obtained by the model and by the FEM simulation for different volume fractions. For the second one, three different meshes have been realised with three different volume fractions (Fig. 8) and the results were obtained by averaging the PP axial stress in the volume of the matrix phase. The SCC is then validated for different volume fractions. One of the advantages of micro-mechanical modelling is their ability to estimate the stress and the strain average in each phase. To illustrate this point stress versus strain has been drawn in Fig. 14 for the HEM and for each phase in a tensile test at a constant strain rate of $0.001\ s^{-1}$. At a given macroscopic strain, the strain of the PP is lower and higher in the rubber. We can observe that for a same macroscopic strain, each phase has different response depending on the rubber volume fraction. It can be concluded that this micro-mechanical model gives interesting results for the two volume fractions considered. Further works will deal with the predictive capacities of such a model.

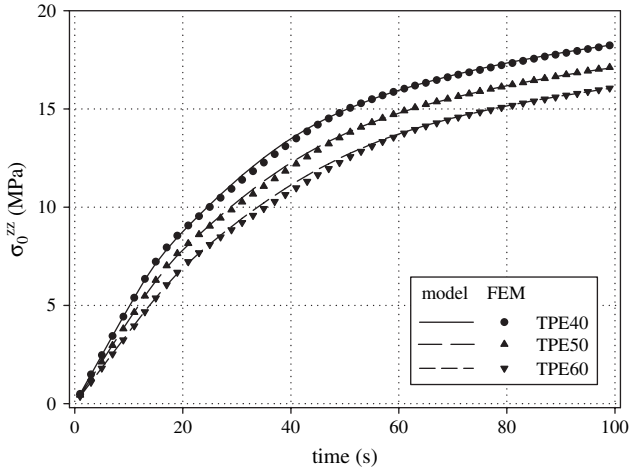

Fig. 13. Comparison of calculated axial stress in the PP obtained by the model and by the FEM simulation for different volume fractions at $\dot{E}^{zz} = 10^{-3}\ s^{-1}$.

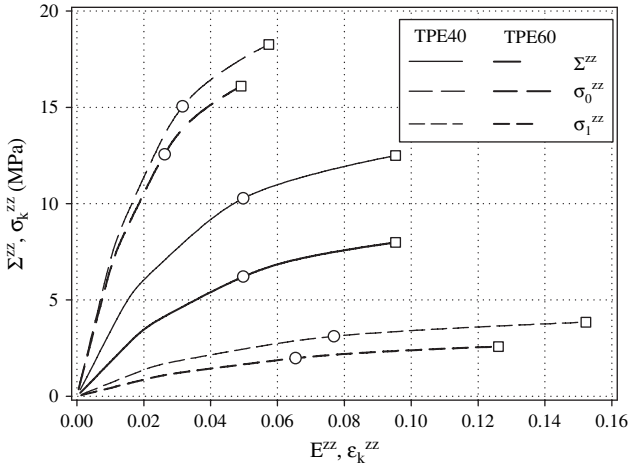

Fig. 14. Simulated Cauchy stress versus logarithmic axial strain in the HEM and in the two phases for TPE40 and TPE60 at $\dot{E}^{zz} = 10^{-3}\ s^{-1}$. Two stages are shown: ○ – $E^{zz} = 0.0497$; □ $E^{zz} = 0.0953$.

5. Conclusion

The aim of this work was to study the ability of a micro-mechanical model to represent mechanical behaviour of TPE materials; therefore the mechanical behaviour of a TPE made with a polypropylene matrix and filled with rubber particles has been studied. The thermoplastic behaviour was modelled with a viscoelastic model and the rubber with a purely linear elastic model. The overall behaviour and local mechanical fields were estimated through a generalized self-consistent scheme. In this scheme a pattern with particles of elastomer included in the thermoplastic matrix was chosen for its ability to properly predict the TPE's Young's modulus versus particle volume fraction. A non-linear model was proposed and successfully compared to experimental tests on two TPE with two different rubber particle volume fractions. A particular transition rule was introduced in the model and tested. This model was implemented into a FEM simulation to calculate stress and strain in the pattern at macroscopic level and in the phases. An inverse method was used for finding model parameters. These parameters were chosen such as the model predictions are comparable to experimental results and such as stress and strain in the phase calculated with the model are similar to those computed with the FEM simulation in average in the phases.

Acknowledgements

This work was partly supported by PAI Procope program from the French government. Special thanks to Erwan Bertevas and Ludovic Ruaudel, former students at Laboratoire de Génie Mécanique et Matériaux and Karoline Vetter, former student at Institut für Allgemeinen Maschinenbau und Kunststofftechnik.

References

[1] Wagenknecht U, Steglich S, Wiessner S, Michael H. Macromol Symp 2005;221:237–45.

[2] Scholz H, Pötschke P, Michael H, Mennig G. Kautsch Gummi Kunstst 2002;55:584–9.
[3] Ismail H, Suryadiansyah. Polym Test 2002;21(4):389–95.
[4] Michael H, Scholz H, Mennig G. Kautsch Gummi Kunstst 1999;52: 510–3.
[5] Van Dommelen JAW, Parks DM, Boyce MC, Brekelmans WAM, Baaijens FPT. J Mech Phys Solids 2003;51(3):519–41.
[6] Bédoui F, Diani J, Régnier G. Polymer 2004;45(7):2433–42.
[7] Bédoui F, Diani J, Régnier G, Seiler W. Acta Mater 2006;54(6): 1513–23.
[8] Nikolov S, Doghri I. Polymer 2000;41(5):1883–91.
[9] Nikolov S, Doghri I, Pierard O, Zealouk L, Goldberg A. J Mech Phys Solids 2002;50(11):2275–302.
[10] Ahzi S, Makradi A, Gregory RV, Edie DD. Mech Mater 2003;35(12): 1139–48.
[11] Makradi A, Ahzi S, Gregory RV, Edie DD. Int J Plast 2005;21(4): 741–58.
[12] Chaouche M, Chaari F. Rhéologie 2004;6:54–62.
[13] Bruselle-Dupend N, Laï D, Feaugas X, Guigon M, Clavel M. Oil Gas Sci Technol 2002;57(2):155–68.
[14] Veenstra H, Verkooijen PCJ, van Lent BJJ, van Dam J, de Boer AP, Nijhof APHJ. Polymer 2000;41(5):1817–26.
[15] Sengers WGF, Sengupta P, Noordermeer JWM, Picken SJ, Gotsis AD. Polymer 2004;45(26):8881–91.
[16] Eshelby JD. Proc R Soc London 1957;A241:376–96.
[17] Masson R, Zaoui A. J Mech Phys Solids 1999;47(7):1543–68.
[18] Molinari A, Ahzi S, Kouddane R. Mech Mater 1997;26(1):43–62.
[19] Mercier S, Jacques N, Molinari A. Int J Solids Struct 2005;42(7): 1923–41.
[20] Feaugas X, Pilvin P, Clavel M. Acta Mater 1997;45(7):2703–14.
[21] Chabert E, Bornert M, Bourgeat-Lami E, Cavaillé J-Y, Dendievel R, Gauthier C, et al. Mater Sci Eng A 2004;381(1–2):320–30.
[22] Mélé P, Marceau S, Brown D, de Puydt Y, Alberola ND. Polymer 2002; 43(20):5577–86.
[23] Wang Q-Z, Lee D-J. Mech Mater 1999;31(11):705–16.
[24] Van Dommelen JAW, Brekelmans WAM, Baaijens FPT. Mech Mater 2003;35(9):845–63.
[25] Sheng N, Boyce MC, Parks DM, Rutledge GC, Abes JI, Cohen RE. Polymer 2005;45(2):487–506.
[26] Asami T, Nitta K-h. Polymer 2004;45(15):5301–6.
[27] Stewart R, Goodship V, Guild F, Green M, Farrow J. Int J Adhes Adhes 2005;25(2):93–9.
[28] Bol M, Reese S. Int J Solids Struct 2006;43(1):2–26.
[29] Sala G, Di Landro L, Cassago D. Mater Des 2002;23(1):21–39.
[30] Matsuoka S-I. J Mater Process Technol 1998;84(1–3):175–80.
[31] Dupend-Bruselle N. Ph.D. thesis, Compiègne; 2000.
[32] Nemat-Nasser S, Hori M. Micromechanics: overall properties of heterogeneous materials. 2nd revision ed. Amsterdam: Elsevier; 1999.
[33] Mura T. Micromechanics of defects in solids. 2nd ed. Dordrecht: Martinus Nijhoff Publishers; 1987.
[34] Christensen RM, Lo KH. J Mech Phys Solids 1979;27(4):315–30.
[35] Kolarik J, Pegoretti A. Polymer 2006;47(1):346–56.
[36] Forest S, Pilvin P. Z Angew Math Mech 1999;79(S1):199–202.
[37] Lemaitre J, Chaboche JL. Mechanics of solid materials. Cambridge: Cambridge University Press; 1990.
[38] Ladeveze P, Rougée P. CR Acad Sci 1985;301(II-13):891–4.
[39] Pilvin P, Feaugas X, Clavel M. In: IUTAM symposium, Sèvres (France); 1995. p. 141–8.
[40] Sauter F, Leclercq S. J Nucl Mater 2003;322(1):1–14.
[41] Saï K, Cailletaud G, Forest S. Mech Mater 2006;38(3):203–17.
[42] Cailletaud G, Pilvin P. Rev Eur Elém Finis 1994;3:515–41.
[43] Drozdov AD, Gupta RK. Int J Eng Sci 2003;41:2335–61.
[44] Pilvin P. In: International seminar on Mécamat, Besançon (France); 1988. p. 155–64.